THE JOURNAL OF BIOLOGICAL CHEMISTRY
Vol. 278, No. 50, Issue of December 12, pp. 50506–50513, 2003

Printed in U.S.A.

Structural Basis for the Function of the N-terminal Domain of the ATPase CopA from *Bacillus subtilis**[S]

Received for publication, July 10, 2003, and in revised form, September 22, 2003
Published, JBC Papers in Press, September 27, 2003, DOI 10.1074/jbc.M307389200

Lucia Banci, Ivano Bertini‡, Simone Ciofi-Baffoni, Leonardo Gonnelli, and Xun-Cheng Su

From the Magnetic Resonance Center CERM and Department of Chemistry, University of Florence, Via Luigi Sacconi 6, 50019, Sesto Fiorentino, Florence, Italy

The solution structure of the N-terminal region (151 amino acids) of a copper ATPase, CopA, from *Bacillus subtilis*, is reported here. It consists of two domains, CopAa and CopAb, linked by two amino acids. It is found that the two domains, which had already been separately characterized, interact one to the other through a hydrogen bond network and a few hydrophobic interactions, forming a single rigid body. The two metal binding sites are far from one another, and the short link between the domains prevents them from interacting. This and the surface electrostatic potential suggest that each domain receives copper from the copper chaperone, CopZ, independently and transfers it to the membrane binding site of CopA. The affinity constants of silver(I) and copper(I) are similar for the two sites as monitored by NMR. Because the present construct "domain-short link-domain" is shared also by the last two domains of the eukaryotic copper ATPases and several residues at the interface between the two domains are conserved, the conclusions of the present study have general validity for the understanding of the function of copper ATPases.

The mechanisms regulating the homeostasis of essential metal ions in living organisms has been the subject of many investigations in the recent past (1–5). Attention was particularly directed toward the reactive and potentially toxic copper, and specific copper uptake and intracellular copper trafficking pathways have been identified (6–11). A critical element of this fascinating machinery for copper homeostasis is represented by the P-type copper-transporting ATPases (12–16). A peculiar feature of this kind of ATPases is that the cytoplasmic N terminus contains one or more domains with a M*XCXX*C metal-binding motifs, depending on the degree of evolution of the organism, *i.e.* superior organisms contain up to six domains, whereas in bacteria up to two domains are present (17). The solution structures, with and without copper(I), of single domains of both bacterial and eukaryotic ATPases have been recently solved (7, 18–20). They all display the same overall structure, formed by two α-helices and four β-strands arranged in a classical "ferredoxin-like" $\beta\alpha\beta\beta\alpha\beta$-fold. The two cysteines of the CXXC motif are exposed on the surface of the protein readily accessible for binding the metal ion. Moreover, cytoplasmic copper chaperones such as Hah1 in humans, Atx1 in *Saccharomyces cerevisiae*, and CopZ in *Bacillus subtilis* and *Enterococcus hirae* bacteria, which deliver copper(I) to ATPases, share the same M*XCXX*C metal binding motif and the same $\beta\alpha\beta\beta\alpha\beta$-fold (21–24). In addition, interaction between the N-terminal region of the copper ATPase Ccc2 from *S. cerevisiae* and Atx1 as well as of the bacterial homologues, the copper ATPase CopA and the chaperone CopZ from *B. subtilis*, was demonstrated by yeast and bacterial two-hybrid assays, respectively (25–27). Complex formation of either Atx1 or CopZ with one N-terminal domain of either Ccc2 or CopA was also confirmed and characterized by *in vitro* NMR studies (28, 29).

The functional role of the multiple domains needs further investigation. Several studies are available on the human ATPases, called also Menkes and Wilson proteins (30–32) because their genetic alteration is responsible of these disease, but none of all these studies completely addressed the role and the inter-correlation of the various domains in the process of copper binding.

To gain further information on this machinery we have, therefore, determined the solution structure of the N-terminal region of the copper ATPase CopA from *B. subtilis*, which contains two soluble metal binding domains. The solution structures of the two isolated domains are available (19, 33). In the present study a protein segment of 151 amino acids, which contains the 2 metal binding domains and 4 other amino acids at the C terminus (CopAab hereafter), was expressed. A mutation in position 46 (S46V) was introduced to have a folded protein construct (33), and the solution structure was solved in its apo form. The interaction with copper(I) and silver(I) has been also investigated. The structural features found here for this system most likely hold for all two domain pumps and for the two domains closest to the membrane when the domains are more than two.

EXPERIMENTAL PROCEDURES

Cloning and Purification—The plasmid for the expression of the N-terminal region of CopA from *B. subtilis* was prepared as previously described (19). The single amino acid substitution was introduced using the QuikChange™ site-directed mutagenesis kit from Stratagene. Sequencing of the engineered DNA fragments was achieved using an automatic sequencer ABI 377. The expression and purification of the protein were performed as previously described (19). The ^{13}C-, ^{15}N-, and ^{15}N-labeled proteins were obtained by growing the cells in the labeled Silantes media *Escherichia coli* OD2-CN and OD2-N (Silentes GmbH), respectively.

Sample Preparation—As a precaution against possible disulfide for-

* This work was supported by European Commission Contract "Structural Proteomics in Europe" QLG2-CT-2002-00988, by the Italian COFIN01 Ministero dell'Istruzione, dell'Università e della Ricerca, and by Ente Cassa di Risparmio di Firenze. The costs of publication of this article were defrayed in part by the payment of page charges. This article must therefore be hereby marked "*advertisement*" in accordance with 18 U.S.C. Section 1734 solely to indicate this fact.

[S] The on-line version of this article (available at http://www.jbc.org) contains Supplemental Fig. 1 and Tables 1–3.

The atomic coordinates and structure factors (code 1P6T) have been deposited in the Protein Data Bank, Research Collaboratory for Structural Bioinformatics, Rutgers University, New Brunswick, NJ (http://www.rcsb.org/).

‡ To whom correspondence should be addressed: CERM and Department of Chemistry, University of Florence, Via Luigi Sacconi 6, Sesto Fiorentino, Florence, Italy 50019. Tel.: 39-55-4574272; Fax: 39-55-4574271; E-mail: bertini@cerm.unifi.it.

TABLE I

Acquisition parameters for NMR experiments performed on apoCopAab from B. subtilis

CA and CB represent carbon alpha and carbon beta, respectively.

Experiments	Acquired data points (nucleus)			Spectral width			n^a	Reference
	t_1	t_2	t_3	F_1	F_2	F_3		
				ppm				
[^{1}H, ^{1}H] NOESY[b]	1024(^{1}H)	2048(^{1}H)		15	15		64	57
[^{1}H, ^{1}H] TOCSY[b]	1024(^{1}H)	2048(^{1}H)		15	15		64	58
^{1}H, ^{15}N HSQC[c]	512(^{15}N)	1024(^{1}H)		40	15		16	59
^{1}H, ^{13}C HSQC[c]	256(^{13}C)	2048(^{1}H)		70	14		16	59
CBCA(CO)NH[d]	136(^{13}C)	56(^{15}N)	2048(^{1}H)	88	40	12	16	60
CBCANH[d]	136(^{13}C)	56(^{15}N)	2048(^{1}H)	88	40	12	16	60
HNCO[d]	80(^{13}C)	40(^{15}N)	1024(^{1}H)	16	40	12	8	60
HN(CA)CO[d]	80(^{13}C)	40(^{15}N)	1024(^{1}H)	16	40	12	16	60
(H)CCH TOCSY[d]	272(^{13}C)	96(^{13}C)	1024(^{1}H)	88	88	12	4	61
CC(CO)NH TOCSY[d]	128(^{15}C)	48(^{15}N)	1024(^{1}H)	88	40	12	16	62
^{15}N-Edited [^{1}H,^{1}H] NOESY[c]	368(^{1}H)	64(^{15}N)	1024(^{1}H)	15	40	15	16	63
^{13}C-Edited [^{1}H,^{1}H] NOESY[c]	320(^{1}H)	80(^{13}C)	1024(^{1}H)	15	80	15	8	63
HNHA[b]	256(^{1}H)	40(^{15}N)	1024(^{1}H)	15	40	15	16	35
HNHB[b]	128(^{1}H)	32(^{15}N)	1024(^{1}H)	15	40	15	32	45

[a] Number of acquired scans.
[b] Data acquired on a 800- or 600-MHz spectrometers.
[c] Data acquired on a 700-MHz spectrometer.
[d] Data acquired on a 500-MHz spectrometer equipped with cryoprobe.

mation due to the presence of C*XX*C motifs, the samples were prepared in a Vac atmosphere nitrogen chamber at room temperature. Protein concentrations were determined using a calculated extinction coefficient of 5360 M^{-1} cm^{-1}. Circular dichroism spectra were collected on a Jasco J-810 spectropolarimeter with a fused quartz cuvettes with a 0.1-cm path length (Merck).

The NMR samples of the apo protein were in 20 mM sodium phosphate buffer, pH 7, 90% H_2O, 10% D_2O. The final protein concentration ranges between 1 and 1.5 mM in the presence of 2 mM dithiothreitol. Approximately 0.6 ml of sample was loaded into high quality NMR tubes that were capped with latex serum caps in the Vac Atmospheres chamber.

NMR Experiments and Structure Calculations—The NMR spectra were acquired on Avance 800, 700, 600, and 500 Bruker spectrometers operating at proton nominal frequencies of 800.13, 700.13, 600.13, and 500.13 MHz, respectively. All the triple resonance (TXI 5-mm) probes used were equipped with Pulsed Field Gradients along the *z* axis. The 500-MHz machine was equipped with a triple resonance cryoprobe.

The NMR experiments recorded on ^{13}C,^{15}N- and ^{15}N-enriched and unlabeled samples are summarized in Table I. All three-dimensional and two-dimensional spectra were collected at 298 K, processed using the standard Bruker software (XWINNMR), and analyzed through the XEASY program (34).

The backbone assignment was performed using the three-dimensional spectra CBCANH, CBCA(CO)NH, HN(CA)CO, HNCO, and HN(CA)CO (CA and CB represent carbon alpha and carbon beta, respectively). The assignment of the aliphatic side chain resonances was performed through the analysis of three-dimensional CC(CO)NH and (H)CCH TOCSY[1] spectroscopy together with ^{15}N-edited NOESY-HSQC and ^{13}C-edited NOESY-HSQC spectra. Distance constraints for structure determination were obtained from ^{15}N-edited and ^{13}C-edited three-dimensional NOESY-HSQC experiments and from two-dimensional NOESY (see Table I). $^3J_{HNH\alpha}$ coupling constants, determined through the HNHA experiment, were transformed into backbone dihedral ϕ angles through the Karplus equation (35). Backbone dihedral ψ angles for residue (i-1) were also determined from the ratio of the intensities of the $d\alpha_N$(i-1,i) and $d_{N\alpha}$(i,i) NOEs obtained from the ^{15}N-edited NOESY-HSQC spectrum. The elements of secondary structure were determined on the basis of the chemical shift index (36), of the $^3J_{HNH\alpha}$ coupling constants, and of the backbone NOEs.

An automated CANDID (37) approach combined with the fast DYANA torsion angle dynamics algorithm was used to assign the ambiguous NOE cross-peaks and to have a preliminary protein structure. Structure calculations were then performed through iterative cycles of DYANA (38) followed by restrained energy minimization (REM) with AMBER 5.0 (39) applied to each member of the family. The quality of the structures was evaluated using the programs PROCHECK-NMR (40) and AQUA (40). The figures were generated with the program MOLMOL (41).

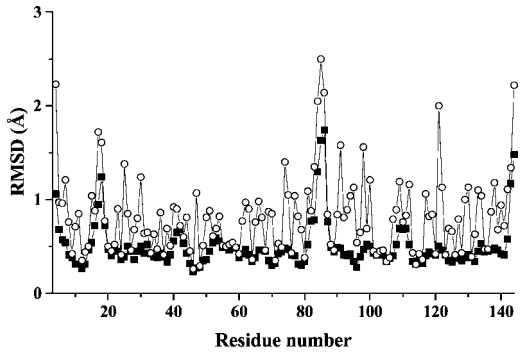

FIG. 1. **r.m.s.d. per residue to the mean structure of apoCopAab (residues 3–144) from *B. subtilis* for the backbone (*filled squares*) and all heavy atoms (*open circles*).**

Relaxation Measurements and Analysis—Relaxation experiments were collected at 298 K on a 1.5 mM sample on a Bruker Avance 600 spectrometer operating at proton nominal frequencies of 600.13 MHz. ^{15}N R_1, R_2, and steady-state heteronuclear NOEs were measured with the gradient-enhanced, sensitivity-enhanced pulse sequences as described by Farrow *et al.* (42). R_2 were measured using refocusing times (τ_{CPMG}) of 450 μs in the Carr-Purcell-Meiboom-Gill (CPMG) detection scheme. All experiments use the "water flipback" scheme to suppress the water signal without its saturation. A recycle delay of 3 s was used for R_1 and R_2. The steady state heteronuclear ^{1}H,^{15}N NOE was obtained by recording spectra with and without proton saturation. In the case of reference spectra without proton saturation, a relaxation delay of 6 s was employed, whereas a delay of 3 s before the proton saturation was employed for spectra with proton saturation. The latter was achieved with a train of 120° ^{1}H pulses at 20-ms intervals.

1024 × 256 data points were collected for each map using 8 scans for each experiment. A spectral window of 40 ppm in the F1 (^{15}N frequency) dimension and of 16 ppm in the F2 (^{1}H frequency) dimension were used. Quadrature detection in F1 was obtained by using the TPPI method. Integration of cross-peaks for all spectra was performed by using the standard routine of the XWINNMR program.

Relaxation rates R_1 and R_2 were determined by fitting the cross-peak intensities measured as a function of the delay within the pulse sequence to a single exponential decay. Errors on the rates were estimated through a Monte Carlo approach. Heteronuclear ^{1}H,^{15}N NOE values were calculated as the ratio of peak volumes in spectra recorded with and without ^{1}H saturation. The heteronuclear ^{1}H,^{15}N NOE values and their errors were estimated by calculating the mean ratio and the S.E. from the available data sets.

[1] The abbreviations used are: TOCSY, total correlation spectroscopy; NOESY, nuclear Overhauser effect (NOE) spectroscopy; HSQC, heteronuclear single quantum coherence; REM, restrained energy minimization; r.m.s.d., root mean square deviation.

TABLE II

Statistical analysis of the REM family and the mean structure of apoCopAab from B. subtilis

REM indicates the energy minimized family of 30 structures; <REM> is the energy-minimized average structure obtained from the coordinates of the individual REM structures.

	REM (30 structures)	<REM>
RSM violations per experimental distance constraint (Å)[a]		
Intraresidue (565)	0.0162 ± 0.0020	0.0153
Sequential (914)	0.0088 ± 0.0014	0.0097
Medium range[b] (742)	0.0154 ± 0.0012	0.0151
Long range (1082)	0.0111 ± 0.0016	0.0110
Total (3303)	0.0127 ± 0.0007	0.0125
ϕ (80) (degree)	0.6697 ± 0.2665	0.939
ψ (72) (degree)	0.1603 ± 0.2616	0.0
Average number of violations per structure		
Intraresidue	18.26 ± 2.83	15
Sequential	9.33 ± 1.97	8
Medium range[b]	19.36 ± 2.25	18
Long range	15.03 ± 3.53	13
Total	62.00 ± 5.00	54
ϕ	1.86 ± 0.99	2
ψ	0.33 ± 0.53	0
Average No. of NOE violations larger than 0.3 Å	0	0
Total NOE square deviations (Å^2)	0.65 ± 0.06	0.65
Average torsion deviations (radian^2)	0.02 ± 0.01	0.02
r.m.s.d. to the mean structure (5–143) (Å)	0.57 ± 0.11 Å (BB) 0.95 ± 0.09 (HA)	
Structural analysis[c]		
% of residues in most favorable regions	75.1	78.3
% of residues in allowed regions	22.2	17.8
% of residues in generously allowed regions	2.5	3.1
% of residues in disallowed regions	1.1	0.8
H-bond energy (kJ mol^{-1})	2.93 ± 0.05	2.92
Overall G-factor	−0.25 ± 0.02	−0.24
Experimental restraints analysis[d]		
% completeness of experimentally observed NOE up to 4 Å cut-off distance	70.5%	66.2%
% completeness of experimentally observed NOE up to 5 Å cut-off distance	49.8%	46.4%

[a] The number of experimental constraints for each class is reported in parenthesis.
[b] Medium range distance constraints are those between residues (i,i + 2), (i,i + 3), (i,i + 4), and (i,i + 5).
[c] As it results from the Ramachandran plot analysis. For the PROCHECK statistics, an average hydrogen bond energy in the range of 2.5–4.0 kJ mol^{-1} and an overall G-factor larger than −0.5 are expected for a good quality structure.
[d] As it results from AQUA analysis.

An estimate of the overall tumbling correlation time and the local correlation times for the NH vector of each residue were derived from the measured R_2/R_1 ratios. In this analysis care was taken to remove from the input the relaxation data of those NHs that have exchange contributions to the R_2 value or which are exhibiting internal motions producing low ^{1}H,^{15}N NOE values.

NMR Titration of the Apo Protein with Cu(I) and Ag(I)—Titrations of ^{15}N-labeled apo protein with copper(I), added as $[(CH_3CN)_4Cu]PF_6$, or silver(I), added as $AgNO_3$, both solved in acetonitrile, were performed by monitoring the ^{1}H,^{15}N HSQC spectral changes upon the addition of increasing amounts of metal ions. Aliquots were added in a Coy chamber under a nitrogen atmosphere at 298 K using a Hamilton syringe to deliver small amounts of metal solution to the labeled samples in NMR tubes. The starting ^{15}N-labeled protein samples were 1.0 or 0.5 mM in concentration. The additions range from 0.2 or 0.1 mM to 3.0 or 2.0 mM in Cu(I), and from 0.2 to 1.6 mM in Ag(I). The metal-bound content was checked through atomic absorption measurements. Three-dimensional NOESY ^{15}N HSQC experiments were recorded on silver(I) samples with protein/metal concentration ratios of 3:1.

Coordinates—The atomic coordinates and structural constraints have been deposited in the Protein Data Bank (accession code 1P6T).

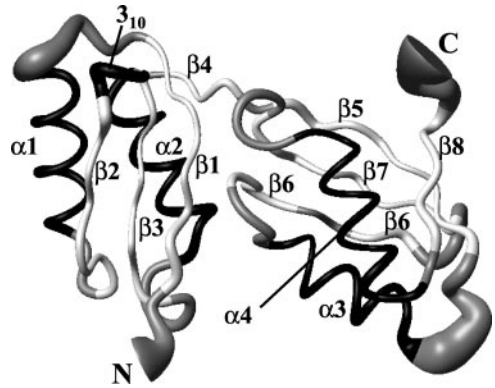

FIG. 2. **30 lowest energy structures of apoCopAab (residues 3–144) from *B. subtilis*, shown as a tube with a radius proportional to the backbone r.m.s.d. value of each residue.** 3_{10}-helix and α-helices are in *black*, and β-strands are in *white*.

RESULTS

CopAab construct contains 2 domains with 40% identity and 2 M*X*C*XX*C copper binding motifs separated by 68 amino acids. *In vivo* this construct is followed by eight transmembrane helices and by the ATP binding and the Actuator domains (30). CopAab construct is structurally characterized in the demetalized form.

NMR Structure of ApoCopAab—The resonance assignment was accomplished by the analysis of triple and double resonance experiments (Table I). 147 of the expected 151 ^{15}N backbone amide resonances were observed and assigned. The amide resonances are missing for residues Met-1, Leu-2, Ala-18, and Ala-86, as they were not determined in the separated domains (19, 33). In total the resonances of 92% of carbon atoms, 96% of nitrogen atoms, and 95% of protons were assigned. These values compare well with those found for the separated domains (19, 33). The ^{1}H, ^{13}C, and ^{15}N resonance assignments of apoCopAab can be found as Supplementary Table 1.

Chemical shift index analysis (36) on Hα, CO, Cα, and Cβ resonances, the $^3J_{HNH\alpha}$ coupling constants, the $d\alpha_N(i\text{-}1,i)/d_{N\alpha}(i,i)$ ratios (43), and the NOEs patterns indicated the presence of eight β strands and four α helices, ordered in two consecutive $\beta\alpha\beta\beta\alpha\beta$ motives, with a 3_{10}-helix between strands β2 and β3, as in the separated domains (19, 33). 5099 NOE

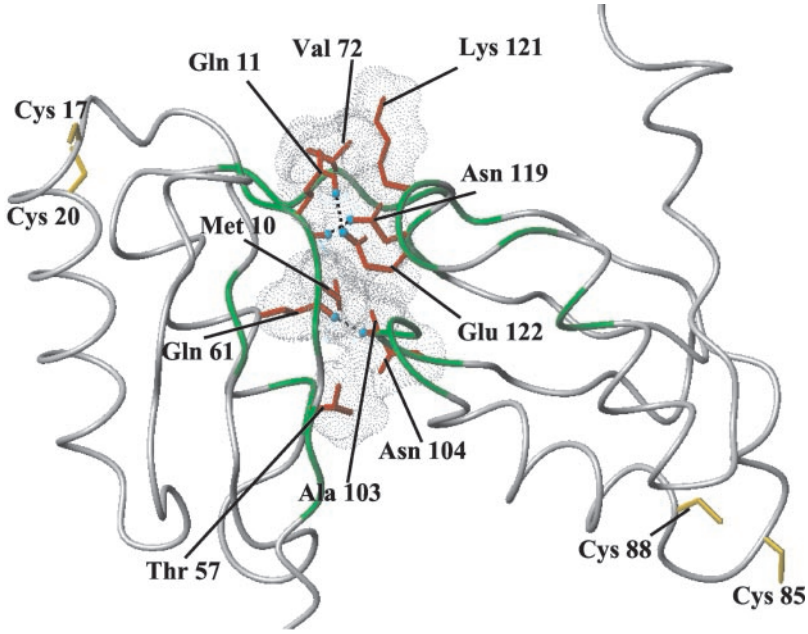

FIG. 3. **Van der Waals contacts at the domain-domain interface of apo-CopAab from *B. subtilis*.** The interacting residues are shown in *red*. The cysteine ligands are shown in *yellow*. Backbone amide resonances experiencing chemical shift differences between the separated domains and the complete N-terminal region are mapped in *green* on the backbone of the structure. Hydrogen bonds at the domain-domain interface of apoCopAab are represented as *black dashed lines*.

cross-peaks were assigned and integrated, providing 4102 unique upper distance limits, of which 3303 are meaningful. 152 angle constraints, 80 ϕ and 72 ψ, were experimentally determined and used in the structure calculations. After REM on each of the 30 conformers of the family, the r.m.s.d. to the mean structure (for residues 5–143) of the conformers of the family is 0.57 ± 0.11 Å for the backbone and 0.95 ± 0.09 Å for all heavy atoms; the penalty is 0.65 ± 0.06 Å^2 for distance constraints and 0.02 ± 0.01 radian^2 for angle constraints. These values compare well with those of the separated domains (19, 33). The r.m.s.d. values per residue to the mean structure of the REM family are shown in Fig. 1. The copper binding loops are the most disordered regions besides the N and C termini. The first in sequence cysteines for each binding site, Cys-17 and Cys-85, are disordered and span variable conformations, whereas the second copper binding cysteines, Cys-20 and Cys-88, located in helices α1 and α3, respectively, have a well defined conformation, identical in both domains. The latter feature is conserved among the apo forms of the metal binding domains of ATPases for which the structure is available (18–20). The statistical analysis of the REM family and the average structure are reported in Table II.

The protein is organized in two domains with the same ferredoxin-like fold but spatially oriented in different ways (Fig. 2). The two domains are linked through only two residues, Val-72 and Thr-73, which connect the last β-strand of the first domain (β4) and the first β-strand of the second domain (β5). The two domains are closely packed to form a single rigid molecule. There are two interacting regions between the two domains, one involving residues 11–12 and 72 with residues 119–122 and the other involving residues 9–10, 57, and 61 with residues 103–104 (Fig. 3). The interdomain interaction surface is experimentally well determined by 22 interdomain QNOEs. The final structure indicates am H-bond network at the interdomain region, involving the following pairs: Hϵ2 Gln-11/Oϵ2 Glu-122, backbone NH Gln-11/Nδ2 Asn-119, and Hδ2 Asn-104/Oϵ1 Gln-61. Hydrophobic contacts are limited to the interactions between Met-10 and Ala-103 and between Val-72 and the side chain of Lys-121, thus indicating that hydrophobic interactions do not play a relevant role in the interdomain contacts. All the residues located in the domain-domain-interacting area experience sizeable chemical shift variations with respect to the separated domains (shown in *green* in Fig. 3). On the contrary, residues located close to the copper binding site of the two domains have small or negligible chemical shift differences, indicating that no perturbation is produced by the presence of the other subunit and that no subunit-subunit interaction is present on this side of the structure, in accordance with the structural data (Fig. 3). The solvent accessibility of the residues at the domain interface shows a dramatic decrease when passing from the isolated domains to the entire construct.

Dynamic Properties of ApoCopAab—Backbone mobility in the subnanosecond time range is homogeneous along the entire polypeptide sequence as it results from ^{15}N relaxation properties determined through ^{15}N R_1, R_2, and ^{1}H,^{15}N NOE measurements (data are reported in Supplementary Fig. 1). Only eight residues (94–98 and 125–127) have R_2 values larger than the average, thus suggesting conformational exchange processes on the ms-μs time scale. Moreover, the C- and N-terminal protein segments display negative NOEs values that suggest a flexibility in the subnanosecond time scale. The average values of R_1, R_2, and ^{1}H,^{15}N NOE, excluding the N- and C-terminal stretches and, as far as R_2 is concerned, the above 8 residues, are 1.14 ± 0.19 s^{-1}, 13.04 ± 1.98 s^{-1}, and 0.80 ± 0.11, respectively. The small range of these values indicate a homogeneous dynamic behavior of the molecule in the subnanosecond time scale. From the R_2/R_1 ratio the overall tumbling correlation time (τ_m) was calculated to be 11.3 ± 1.1 ns. This value is consistent with the molecular mass of this protein according to the Stokes-Einstein relation (44), and it is almost twice that found for the two isolated domains (29, 33). This result indicates that the two domains are rigidly held one with respect to the other.

Interaction of ApoCopAab with Metal Ions—The interaction of apoCopAab with copper(I) and silver(I) ions was studied through NMR titrations by monitoring chemical shift variations of the amide resonances in ^{1}H,^{15}N HSQC experiments. Initial additions of copper(I) (up to a copper/protein ratio equal to 0.5) to a 1.0 mM solution of apoCopAab produce a significant line broadening, in some cases beyond detection, of some amide resonances close to each metal binding site (*i.e.* Thr-16, Thr-84, Ala-21, Ala-89, and the Cys ligands), whereas the majority of amide resonances remains unperturbed. Further additions of copper(I) up to copper/protein ratio equal to 1.0 (*i.e.* 0.5 eq/metal binding site) cause the appearance of new NH peaks (Thr-16, Thr-84, Ala-21, and Ala-89) with chemical shift values

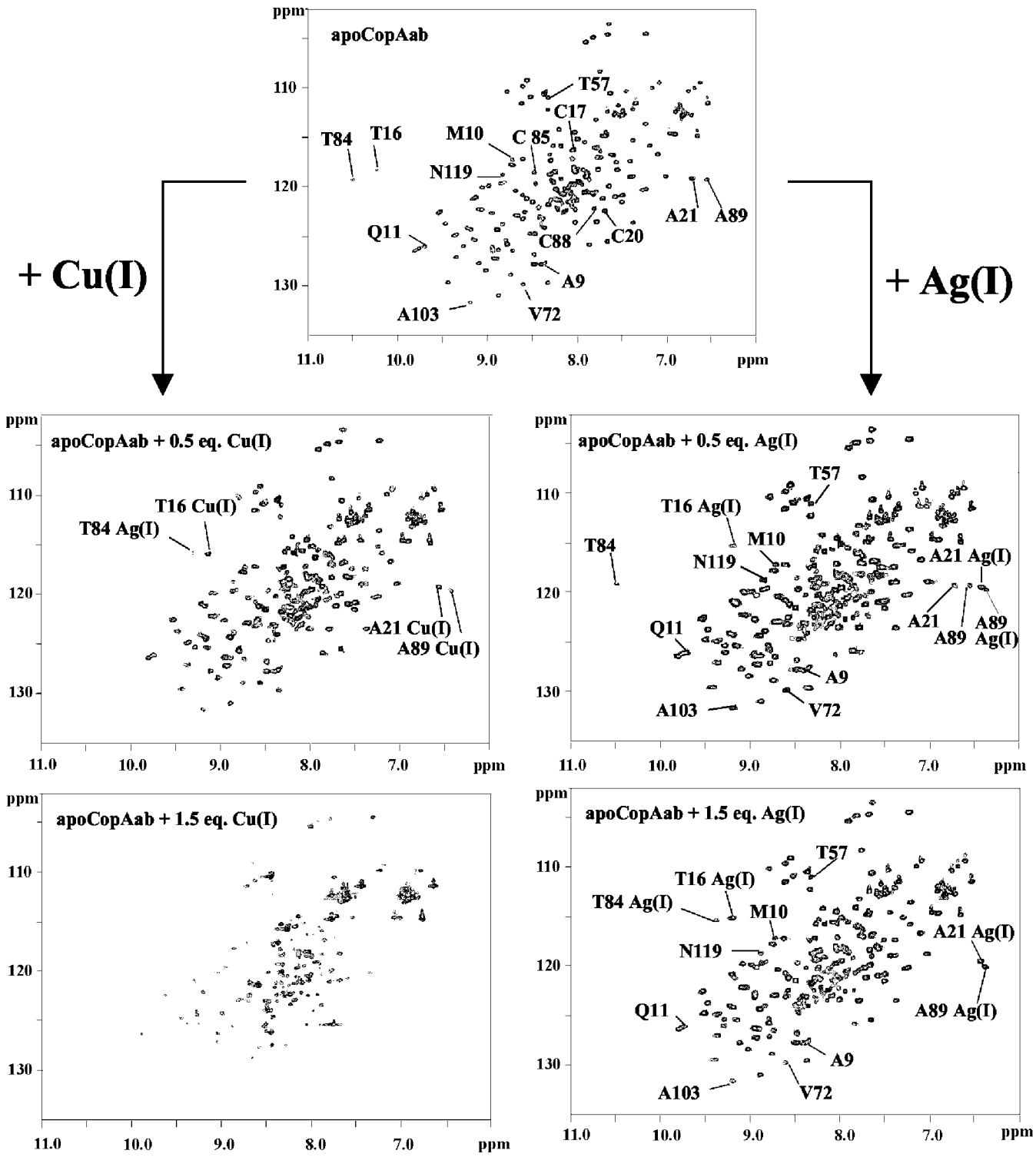

FIG. 4. **$^{1}H,^{15}N$ HSQC spectra (700 MHz, 298 K) of apoCopAab in the presence of 0, 0.5, and 1.5 eq/metal binding site of Cu(I) and Ag(I).** The initial protein concentrations are 1 and 0.5 mM for Cu(I) and Ag(I) titrations, respectively.

very close to those observed in the Cu(I) form of each isolated domain (Fig. 4). This might indicate that the two domains bind copper(I) with a similar affinity. Furthermore, it appears that Cu(I) binding to both metal binding sites is occurring with slow/intermediate exchange rates on the NMR time scale. Further additions of copper(I) (up to a copper/protein ratio equal to 3.0, *i.e.* 1.5 eq/per metal binding site) determine the disappearance/broadening of most of NH signals in the $^{1}H,^{15}N$ HSQC spectra (Fig. 4). These effects exclusively originate from copper binding and are reversible; when copper is removed with a very high affinity copper(I) ligand such as bathocuproine disulfonate, the spectra of the apo form are completely recovered. When the titration with copper(I) is performed using half-concentration of protein with respect to the first titration, the resonances in the $^{1}H,^{15}N$ HSQC spectrum of CopAab with a copper/protein ratio equal to 3.0 are largely conserved even if with weaker intensity with respect to the spectra of the apo form. Therefore, the line broadening of the backbone NH resonances is not only copper-dependent, but also protein concentration-dependent.

Line broadening up to the complete disappearance of the

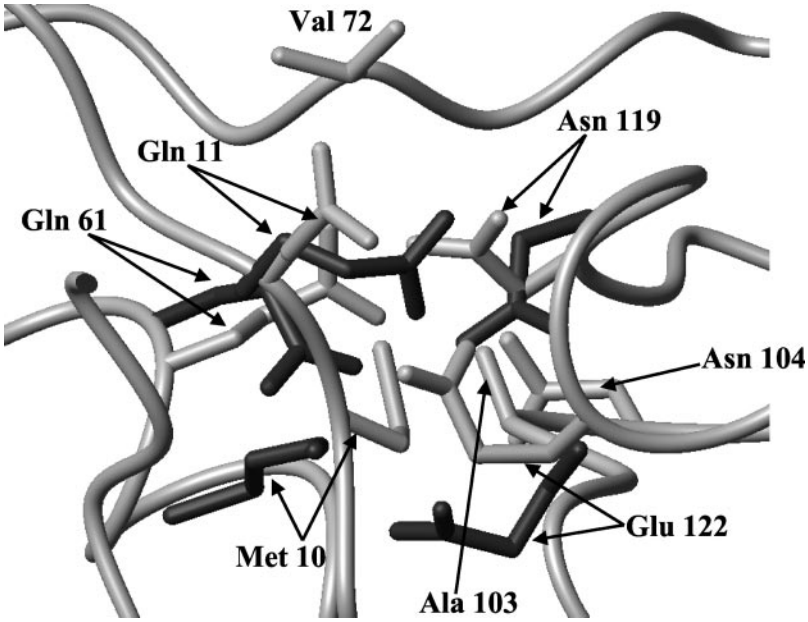

FIG. 5. **Some residues involved in the domain-domain interactions are shown for both apoCopAab (*gray*) and the isolated apoCopAa and apoCopAb domains (b*lack*).**

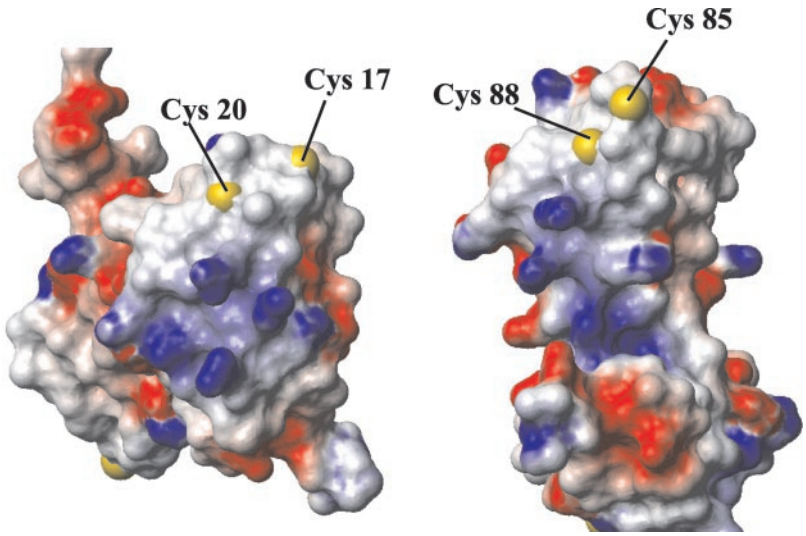

FIG. 6. **Electrostatic potential surfaces of apoCopAab orientated in such a way to show the copper binding sites.** The positively and negatively charged and neutral amino acids are represented in *blue*, *red*, and *white*, respectively. The Cys ligands are also shown in *yellow*.

^{15}NH signals can be due to molecular aggregation induced by the coordination properties of copper(I), which prefers a three/four-coordination state. A similar phenomenon was observed in the case of Cu(I)CopZ from *E. hirae* (24). Because aggregation does not occur within separated domains upon copper binding, the interaction probably occurs between different domains.

A further titration was performed using Ag(I), which adapts a similar coordination state and for this reason is sometimes used as a substitute of copper(I) (20). The ^{1}H,^{15}N HSQC spectra performed during the titration show that NHs resonances close to both metal binding sites, with characteristic shifts of the apo form, disappear with the concomitant formation of new peaks, which are due to the silver(I)-bound form (Fig. 4). The latter form is characterized by chemical shifts very similar to those found for the copper(I)-bound form of the two isolated domains. No significant line broadening occurs (Fig. 4). The analysis of the ^{1}H,^{15}N HSQC together with a three-dimensional NOESY-HSQC experiment shows that the chemical shifts of the backbone NHs of all residues belonging to the interdomain interaction region are not strongly affected by the presence of silver(I) (Fig. 4), suggesting that the binding of the silver(I) does not determine significant relative structural rearrangements of the two domains.

During the titration of the apo protein with silver(I), the variation in the normalized intensities of the signal of Ala-21 of the first domain and of Ala-89 of the second domain were followed with respect to [Ag(I)]. At a 1:1 [Ag(I)]/[CopAab] ratio, the first domain is metalized for about 60%, whereas the second domain is metalized for about 40%. The metal binding site of the first domain results completely saturated at a 2:1 [Ag(I)]/[CopAab] ratio, whereas the other domain required a slight excess of silver(I) to obtain a fully metalized state. This behavior provides evidence that the first domain has an affinity constant $>10^{4}$ M^{-1}, whereas the second has a slightly lower affinity.

DISCUSSION

A comparison between the structure of apoCopAab with that of the two separated domains shows an essentially identical overall fold and length of secondary structure elements, with global backbone r.m.s.d. values with the first and second isolated domains of 1.2 and 1.5 Å, respectively. All the secondary structure elements and loops are well superimposed. However, the apoCopAab structure experiences meaningful differences with respect to the isolated apoCopAa and apoCopAb structures, specifically in the side chain conformation of some resi-

dues at the interdomain interface, Met-10, Gln-11, Gln-61, Asn-119, and Glu 122 (Fig. 5). From the isolated domains to the double domain construct Met-10 moves from the interior of the protein core toward the interaction surface in the vicinity of Ala-103, and Gln-61 moves to approach the side chain of Asn-104 to form a H-bond with it. The side chains of the other residues display structural rearrangements to favor the domain-domain interactions (Fig. 5).

Gln-11 forms hydrogen bonds with Asn-119 and Glu-122, which connect the two domains. Sequence analysis of the fifth and sixth domains of all mammal copper transporting ATPases indicates that these two domains are always connected by a short stretch formed by only a few amino acids and that a Gln residue is always conserved in the sequence position corresponding to Gln-11 for the fifth domain, and Asp and Glu residues are always conserved in place of Asn-119 and Glu-122 for the sixth domain (17, 19). Therefore, it may be suggested that a hydrogen bond network, which connects the fifth and sixth domains, is conserved also in the superior organisms in humans and constitutes a key structural element for the domain interactions.

The solution structure of apoCopAab as well as its dynamic properties show that the two domains are closely packed to form a single rigid molecule, with both metal binding sites easily accessible. Therefore, considering that a functional relation between CopA and CopZ from *B. subtilis* has been recently detected *in vivo* (27) and protein-protein interaction has been characterized *in vitro* (29), it is reasonable to conclude that the protein partner CopZ can release copper(I) to both metal binding sites independently. The partner protein-protein interaction was shown to occur between the negatively charged surface of CopZ and the positive surface of the second domain of CopA (29). Both domains of apoCopAab have an accessible positively charged region (Fig. 6); thus, both have the possibility of interacting with the partner CopZ.

Interaction with Metal Ions and Related Biological Implications—The copper:protein stoichiometry of the Wilson and the Menkes copper binding N-terminal domains was extensively characterized (46–48). A recent paper (49) reports that each domain is capable to bind copper or silver but that the array of six tethered domains binds four equivalents of Cu(I) to produce a monomer containing four Cu(I) ions in a solvent-shielded environment. According to the authors (49), this suggests that a tertiary structural reorganization of the domains makes interdomain copper(I) interactions possible. These conformational changes may act *in vivo* as a trigger for the translocation of the protein from the trans-Golgi network to the plasma membrane or to a vacuolar compartment (50, 51). Furthermore, the N-terminal region of the Wilson protein is shown to interact with the ATP binding domain (52). In the copper-bound form such interaction is weakened, determining an increase in affinity of ATP for the ATP binding domain (52), thus triggering the copper translocation process. A similar functional role for the N-terminal domains has been also proposed for other ATPases (53, 54).

The present studies and the interaction of CopAab with copper(I) and silver(I) together with the solution structure of the apo form and its dynamic properties suggests that the two domains, which both have positively charged, solvent-exposed patches, are organized to receive copper independently one from the other from its copper chaperone partner, CopZ, to start the metal transfer process. Our data fit within a model proposed for the function of the Wilson protein *in vivo* (51, 55), where the binding of copper to the domains closest to the transmembrane segments is the first step of the copper transport cycle, sufficient for the basic activity and for the delivery of copper to the multicopper oxidase target. When the copper concentration increases, other metal binding sites become occupied, thus inducing conformational changes that determine the translocation process of the Wilson protein from the trans-Golgi network to the plasma membrane. This model could also explain the reason why eukaryotic organisms have developed a higher number of domains that are needed to activate the protein translocation process, whereas the bacterial ATPases have only one or two domains since they do not have internal organelles, and therefore, translocation processes are not required. It has been also observed that, in copper(I) ATPases with multiple copper binding domains, those closest to the transmembrane region appear to be functionally more important than those closest to the N terminus for the copper transport function (50, 56). Our data show that the two domains close to the transmembrane region do not interact with each other and that there are no significant conformational changes upon metal binding. They presumably transfer copper to residues within the channel for subsequent translocation across the membrane without playing an important role in the protein translocation process.

REFERENCES

1. Finney, L. A., and O'Halloran, T. V. (2003) *Science* **300,** 931–936
2. Puig, S., and Thiele, D. J. (2002) *Curr. Opin. Chem. Biol.* **6,** 171–180
3. Maroney, M. J. (1999) *Curr. Opin. Chem. Biol.* **3,** 188–199
4. Eide, D. (1997) *Curr. Opin. Cell Biol.* **9,** 573–577
5. Andrews, N. C. (2002) *Curr. Opin. Chem. Biol.* **6,** 181–186
6. Banci, L., and Rosato, A. (2003) *Acc. Chem. Res.* **36,** 215–221
7. Opella, S. J., DeSilva, T., and Veglia, G. (2002) *Curr. Opin. Struct. Biol.* **6,** 217–223
8. O'Halloran, T. V., and Culotta, V. C. (2000) *J. Biol. Chem.* **275,** 25057–25060
9. Pena, M. M. O., Lee, J., and Thiele, D. J. (1999) *J. Nutr.* **129,** 1251–1260
10. Rosen, B. P. (1999) *Essays Biochem.* **34,** 1–15
11. Vulpe, C. D., and Packman, S. (1995) *Annu. Rev. Nutr.* **15,** 293–322
12. Rensing, C., Fan, B., Sharma, R., Mitra, B., and Rosen, B. P. (2000) *Proc. Natl. Acad. Sci. U. S. A.* **97,** 652–656
13. Solioz, M., and Vulpe, C. D. (1996) *Trends Biochem. Sci.* **21,** 237–241
14. Vulpe, C. D., Levinson, B., Whitney, S., Packman, S., and Gitschier, J. (1993) *Nat. Genet.* **3,** 7–13
15. Chelly, J., Tumer, Z., Tonnesen, T., Petterson, A., Ishikawa-Brush, Y., Tommerup, N., Monaco, A. P., and Horn, N. (1993) *Nat. Genet.* **3,** 14–19
16. Bull, P. C., Thomas, G. R., Rommens, J. M., Forbes, J. R., and Cox, D. W. (1993) *Nat. Genet.* **5,** 327–337
17. Arnesano, F., Banci, L., Bertini, I., Ciofi-Baffoni, S., Molteni, E., Huffman, D. L., and O'Halloran, T. V. (2002) *Genome Res.* **12,** 255–271
18. Banci, L., Bertini, I., Ciofi-Baffoni, S., Huffman, D. L., and O'Halloran, T. V. (2001) *J. Biol. Chem.* **276,** 8415–8426
19. Banci, L., Bertini, I., Ciofi-Baffoni, S., D'Onofrio, M., Gonnelli, L., Marhuenda-Egea, F. C., and Ruiz-Dueñas, F. J. (2002) *J. Mol. Biol.* **317,** 415–429
20. Gitschier, J., Moffat, B., Reilly, D., Wood, W. I., and Fairbrother, W. J. (1998) *Nat. Struct. Biol.* **5,** 47–54
21. Wernimont, A. K., Huffman, D. L., Lamb, A. L., O'Halloran, T. V., and Rosenzweig, A. C. (2000) *Nat. Struct. Biol.* **7,** 766–771
22. Arnesano, F., Banci, L., Bertini, I., Huffman, D. L., and O'Halloran, T. V. (2001) *Biochemistry* **40,** 1528–1539
23. Banci, L., Bertini, I., Del Conte, R., Markey, J., and Ruiz-Dueñas, F. J. (2001) *Biochemistry* **40,** 15660–15668
24. Wimmer, R., Herrmann, T., Solioz, M., and Wüthrich, K. (1999) *J. Biol. Chem.* **274,** 22597–22603
25. Pufahl, R. A., Singer, C. P., Peariso, K. L., Lin, S.-J., Schmidt, P. J., Fahrni, C. J., Cizewski Culotta, V., Penner-Hahn, J. E., and O'Halloran, T. V. (1997) *Science* **278,** 853–856
26. Portnoy, M. E., Rosenzweig, A. C., Rae, T., Huffman, D. L., O'Halloran, T. V., and Cizewski Culotta, V. (1999) *J. Biol. Chem.* **274,** 15041–15045
27. Radford, D. S., Kihlken, M. A., Borrelly, G. P. M., Horwood, C. R., Le Brun, N. E., and Cavet, J. S. (2003) *FEMS Microbiol. Lett.* **220,** 105–112
28. Arnesano, F., Banci, L., Bertini, I., Cantini, F., Ciofi-Baffoni, S., Huffman, D. L., and O'Halloran, T. V. (2001) *J. Biol. Chem.* **276,** 41365–41376
29. Banci, L., Bertini, I., Ciofi-Baffoni, S., Del Conte, R., and Gonnelli, L. (2003) *Biochemistry* **42,** 1939–1949
30. Lutsenko, S., Efremov, R. G., Tsivkovskii, R., and Walker, J. M. (2002) *J. Bioenerg. Biomembr.* **34,** 351–362
31. Fatemi, N., and Sarkar, B. (2002) *J. Bioenerg. Biomembr.* **34,** 339–349
32. Voskoboinik, I., and Camakaris, J. (2002) *J. Bioenerg. Biomembr.* **34,** 363–371
33. Banci, L., Bertini, I., Ciofi-Baffoni, S., Gonnelli, L., and Su, X. C. (2003) *J. Mol. Biol.* **331,** 473–484
34. Eccles, C., Güntert, P., Billeter, M., and Wüthrich, K. (1991) *J. Biomol. NMR* **1,** 111–130
35. Vuister, G. W., and Bax, A. (1993) *J. Am. Chem. Soc.* **115,** 7772–7777
36. Wishart, D. S., and Sykes, B. D. (1994) *J. Biomol. NMR* **4,** 171–180
37. Herrmann, T., Güntert, P., and Wüthrich, K. (2002) *J. Mol. Biol.* **319,** 209–227
38. Güntert, P., Mumenthaler, C., and Wüthrich, K. (1997) *J. Mol. Biol.* **273,** 283–298
39. Pearlman, D. A., Case, D. A., Caldwell, J. W., Ross, W. S., Cheatham, T. E.,

Ferguson, D. M., Seibel, G. L., Singh, U. C., Weiner, P. K., and Kollman, P. A. (1997) *AMBER 5.0*, University of California, San Francisco
40. Laskowski, R. A., Rullmann, J. A. C., MacArthur, M. W., Kaptein, R., and Thornton, J. M. (1996) *J. Biomol. NMR* **8,** 477–486
41. Koradi, R., Billeter, M., and Wüthrich, K. (1996) *J. Mol. Graph.* **14,** 51–55
42. Farrow, N. A., Muhandiram, R., Singer, A. U., Pascal, S. M., Kay, C. M., Gish, G., Shoelson, S. E., Pawson, T., Forman-Kay, J. D., and Kay, L. E. (1994) *Biochemistry* **33,** 5984–6003
43. Gagne, R. R., Tsuda, S., Li, M. X., Chandra, M., Smillie, L. B., and Sykes, B. D. (1994) *Protein Sci.* **3,** 1961–1974
44. Einstein, A. (1956) *Investigations on the Theory of the Brownian Movement*, Dover, New York
45. Archer, S. J., Ikura, M., Torchia, D. A., and Bax, A. (1991) *J. Magn. Reson.* **95,** 636–641
46. DiDonato, M., Narindrasorasak, S., Forbes, J. R., Cox, D. W., and Sarkar, B. (1997) *J. Biol. Chem.* **272,** 33279–33282
47. Lutsenko, S., Petrukhin, K., Cooper, M. J., Gilliam, C. T., and Kaplan, J. H. (1997) *J. Biol. Chem.* **272,** 18939–18944
48. Ralle, M., Cooper, M. J., Lutsenko, S., and Blackburn, N. J. (1998) *J. Am. Chem. Soc.* **120,** 13525–13526
49. Cobine, P. A., George, G. N., Winzor, D. J., Harrison, M. D., Mogahaddas, S., and Dameron, C. T. (2000) *Biochemistry* **39,** 6857–6863
50. Forbes, J. R., Hsi, G., and Cox, D. W. (1999) *J. Biol. Chem.* **274,** 12408–12413
51. DiDonato, M., Hsu, H. F., Narindrasorasak, S., Que, L. J., and Sarkar, B. (2000) *Biochemistry* **39,** 1890–1896
52. Tsivkovskii, R., MacArthur, B. C., and Lutsenko, S. (2001) *J. Biol. Chem.* **276,** 2234–2242
53. Wei, Y., Marchi, V., Wang, R., and Rao, R. (1999) *Biochemistry* **38,** 14534–14541
54. Kuhlbrandt, W., Zeelen, J., and Dietrich, J. (2002) *Science* **297,** 1692–1696
55. Fatemi, N., and Sarkar, B. (2002) *Inorg. Chim. Acta* **339,** 179–187
56. Strausak, D., La Fontaine, S., Hill, J., Firth, S. D., Lockhart, P. J., and Mercer, J. F. (1999) *J. Biol. Chem.* **274,** 11170–11177
57. Wider, G., Macura, S., Kumar, A., Ernst, R. R., and Wüthrich, K. (1984) *J. Magn. Reson.* **56,** 207–234
58. Bax, A., and Davis, D. G. (1985) *J. Magn. Reson.* **65,** 355–360
59. Bodenhausen, G., and Ruben, D. J. (1980) *Chem. Phys. Lett.* **69,** 185–188
60. Kay, L. E., Ikura, M., Tschudin, R., and Bax, A. (1990) *J. Magn. Reson.* **89,** 496–514
61. Kay, L. E., Xu, G. Y., Singer, A. U., Muhandiram, D. R., and Forman-Kay, J. D. (1993) *J. Magn. Reson. B* **101,** 333–337
62. Gardner, K. H., Konrat, R., Rosen, M. K., and Kay, L. E. (1996) *J. Biomol. NMR* **8,** 351–356
63. Wider, G., Neri, D., Otting, G., and Wüthrich, K. (1989) *J. Magn. Reson.* **85,** 426–431

Structural Basis for the Function of the N-terminal Domain of the ATPase CopA from *Bacillus subtilis*

Lucia Banci, Ivano Bertini, Simone Ciofi-Baffoni, Leonardo Gonnelli and Xun-Cheng Su

J. Biol. Chem. 2003, 278:50506-50513.
doi: 10.1074/jbc.M307389200 originally published online September 27, 2003
